Stocchi, P.; Vacchi, M.; Lorscheid, T.; de Boer, B.; Simms, A.R.; van de Wal, R.S.W.; Vermeersen, B.L.A.; Pappalardo, M. & Rovere, A. (2018). MIS 5e relative sea-level changes in the Mediterranean Sea: Contribution of isostatic disequilibrium. *Quaternary Science Reviews*, 185, 122-134

Published version: https://doi.org/10.1016/j.quascirev.2018.01.004

Link NIOZ Repository: www.vliz.be/imis?module=ref&refid=295030

MIS 5e relative sea-level changes in the Mediterranean Sea: contribution of isostatic disequilibrium

Paolo Stocchi[1,*], Matteo Vacchi[2,3], Thomas Lorscheid[4,5], Bas de Boer[6], Alexander R. Simms[7], Roderik van de Wal[6], Bert L.A. Vermeersen[8,9], Marta Pappalardo[10], Alessio Rovere[4,5]

[1]NIOZ - Royal Netherlands Institute for Sea Research, Coastal Systems (TX), and Utrecht University, P.O. Box 59, 1790 AB, Den Burg, Texel, The Netherlands
[2]Université P. Valéry Montpellier 3, CNRS ASM, UMR 5140, 34970 Montpellier, France
[3]Geography, College of Life and Environmental Sciences, University of Exeter, Exeter EX44RJ, UK.
[4]MARUM - Center for Marine Environmental Sciences, University of Bremen, Leobener Straße 8, 28359, Bremen, Germany
[5]ZMT - Leibniz Centre for Tropical Marine Research, Fahrenheitstraße 6, 28359 Bremen, Germany
[6]IMAU – Institute for Marine and Atmospheric research Utrecht, Utrecht University, Utrecht, The Netherlands
[7]University of California Santa Barbara, Santa Barbara (CA), USA
[8]NIOZ - Royal Netherlands Institute for Sea Research, Estuarine and Deltaic Systems (YK), and Utrecht University, Korringaweg 7, 4401 NT, Yerseke, The Netherlands
[9]TU Delft, Faculty of Aerospace Engineering, Delft, The Netherlands
[10]Università di Pisa, Dipartimento di Scienze della Terra, Pisa, Italy

[*]Corresponding author

Abstract

Sea-level indicators dated to the Last Interglacial, or Marine Isotope Stage (MIS) 5e, have a twofold value. First, they can be used to constrain the melting of Greenland and Antarctic Ice Sheets in response to global warming scenarios. Second, they can be used to calculate the vertical crustal rates at active margins. For both applications, the contribution of glacio- and hydro-isostatic adjustment (GIA) to vertical displacement of sea-level indicators must be calculated. In this paper, we re-assess MIS 5e sea-level indicators at 11 Mediterranean sites that have been generally considered tectonically stable or affected by mild tectonics. These are found within a range of elevations of 2-10 m above modern mean sea level. Four sites are characterized by two separate sea-level stands, which suggest a two-step sea-level highstand during MIS 5e. Comparing field data with numerical modeling we show that (i) GIA is an important contributor to the spatial and temporal variability of the sea-level highstand during MIS 5e, (ii) the isostatic imbalance from the melting of the MIS 6 ice sheet can produce a >2.0 m sea-level highstand, and (iii) a two-step melting phase for the Greenland and Antarctic Ice Sheets reduces the differences between observations and predictions. Our results show that assumptions of tectonic stability on the basis of the MIS 5e records carry intrinsically large uncertainties, stemming either from uncertainties in field data and GIA models. The latter are propagated to either Holocene or Pleistocene sea-level reconstructions if tectonic rates are considered linear through time.

Keywords: Pleistocene; Sea Level changes; Europe; Geomorphology, coastal

1. Introduction

Sea-level changes are primarily a reflection of water mass transfer between continents, where water is stored as ice during cold periods, and oceans, where meltwater is introduced during warmer periods. This process is known as glacial eustasy (Suess, 1906) and occurs in response to changes in atmosphere and ocean temperatures related to variations in atmospheric CO_2 concentrations and Milankovitch-driven insolation (Stocker et al., 2013). A fundamental aspect for the study of past climate change over glacial-interglacial time scales is the collection, analysis and interpretation of

Relative Sea Level (RSL) indicators, that are fossil landforms, deposits or biological assemblages with a known relationship with a paleo sea level (Hibbert et al., 2016; Rovere et al., 2016a). Once vertical movements associated with Glacial Isostatic Adjustment (GIA) (Lambeck and Purcell, 2005), tectonics (Simms et al., 2016) or other post-depositional processes (Rovere et al., 2016b) are taken into account, paleo RSL indicators can be used to constrain ice-mass variations in response to changes in atmospheric and ocean temperatures during past interglacials (Dutton et al., 2015). In turn, estimates of paleo global mean sea level can be used to constrain processes regulating ice melting in paleo ice-sheet models, which eventually may be used to gauge the sensitivity of present-day polar ice sheets to future scenarios of global warming (e.g. DeConto and Pollard, 2016).

The most studied past interglacial is the Marine Isotopic Stage 5e (MIS 5e, 117-127 ka), which is the last period of the Earth's history when climate was warmer than today. Generally, MIS 5e sea-level studies are oriented towards two main goals. The first is to understand how to account for processes causing departures from eustasy (e.g., GIA, tectonics) in order to produce reliable estimates of past global mean sea levels. The second consists on the calculation of tectonic movements starting from the elevation of RSL indicators and assumptions on eustatic sea-level changes. This aspect is particularly relevant for the understanding of the long-term vertical movement of coastal areas, which is in turn important for the planning of coastal infrastructures in active geodynamic settings and need to be accounted for to correct future climate-related rates of RSL change (Antonioli et al., 2017).

Despite the common consideration in isolation, the two aims outlined above are mutually dependent and they are both tied to GIA predictions. In fact, to achieve the second goal, one must calculate the climate-related and GIA-modulated RSL elevations, which are the result of the first goal. The latter, however, stems from *a priori* information on long-term tectonic motions, which is the result of this second goal. Studies on MIS 5e RSL change in the Mediterranean Sea have often either adopted standard ESL values to calculate vertical tectonic rates at active sites or neglected the GIA overprint in the calculation of the ESL signal (Ferranti et al., 2006).

In this paper we focus on MIS 5e sea-level variations in the Mediterranean Sea. We investigate the GIA contributions to the spatiotemporal variability of RSL change during MIS 5e within the basin using GIA numerical simulations that incorporate the solid Earth and gravitational response to three glacial-interglacial cycles prior to MIS 5e and that evolve towards present. We also evaluate the GIA-modulated contribution of four scenarios for GrIS and AIS melting during MIS 5e. We compare our RSL predictions to observations from 11 sites that have been previously hypothesized as tectonically stable based on the low elevation of the MIS 5e shoreline.

We use field data and numerical GIA predictions at these sites to address the following questions:

1. How much of the observed MIS 5e RSL variability in the Mediterranean can be explained by GIA?
2. How significant are the uncertainties in GIA, as well as GrIS and AIS melting scenarios when using MIS 5e shorelines to calculate tectonic vertical motions?

2.Materials and methods

2.1 Paleo Relative Sea-level indicators

The Mediterranean Sea has been a central focus for studies on sea level changes for over two centuries (Benjamin et al., 2017). The basin is characterized by different tectonic regimes (Figure 1, see Supplementary Text for a brief outline) and its relatively low tidal amplitudes and low wave energy helped to preserve RSL indicators almost ubiquitously (see Figure 1 in Ferranti et al., 2006 for an overview and detailed reports in Anzidei et al., 2014; Ferranti et al., 2006; Galili et al., 2007; Mauz et al., 2012; Pedoja et al., 2014).

In the absence of MIS 5e reefs (Dutton and Lambeck, 2012; Hibbert et al., 2016), the main Mediterranean Pleistocene RSL indicators can be divided into three main categories: i) Depositional, consisting mostly of cemented beach or shallow marine deposits (Figure 2a-c,e,f). ii) Biological, consisting of fossil remains of benthic organisms living attached to hard substrates (Rovere et al., 2015) or traces of bioeroding organisms (e.g. *L. lithophaga* boreholes, Figure 2d). iii) Geomorphological: all landforms formed by the action of the sea over time. Typical geomorphological MIS 5e markers include fossil shore platforms or tidal notches (Figure 2d, f, Antonioli et al., 2015). Often, dating of Mediterranean MIS 5e RSL indicators is challenging because the preservation of *in situ* corals for U-series measurements is rare.

To calculate the paleo RSL from the measured elevation of a RSL indicator, it is essential to decouple the actual measured elevation of the indicator and the interpretation of the paleo sea level that it represents (Düsterhus et al., 2016). This is done by subdividing the measured elevation, which should be done at the highest possible accuracy and should always be referenced to a tidal datum, and the indicative meaning of the RSL indicator (Shennan, 1982,1989; Hijma et al., 2015; Shennan et al., 2014; Shennan and Horton, 2002; Van de Plassche, 1986). The indicative meaning is composed of the indicative range (IR, the range over which an indicator forms, e.g. from the uppermost tide to the mean lowest tide) and the reference water level (RWL, the midpoint of the indicative range) (see Vacchi et al., 2016 for examples on Holocene Mediterranean RSL indicators). In this study, we assess the elevation and indicative meaning of MIS 5e RSL indicators from 11 sites among the most representative for the Mediterranean (Figure 1). To calculate paleo RSL from the elevation of RSL indicators we followed the approach and formulas suggested by Rovere et al., 2016a. Figure 2 shows geological sketches (a-f) and pictures of sites 5,6 and 11 (f,d,b, respectively). In the Supplementary Materials, we present a spreadsheet with details on how the indicative meaning has been calculated at each site and a text file including an example of paleo RSL calculation for Cala Mosca (site 8, Figure 2c). At sites 3 and 6 the elevation was re-measured with high-accuracy differential GPS (Trimble ProXRT receiver and Trimble Tornado antenna receiving OmniSTAR HP+G2 real-time corrections) and referred to mean sea level using local tidal datums. For the remaining sites, the elevation of the RSL indicators and its accuracy were extracted from published data.

2.2 Glacial- and hydro-isostatic adjustment (GIA)

The GIA process is formally described by the linear and integral Sea Level Equation (SLE; Farrell and Clark, 1976). Solving the SLE for a prescribed ice-sheet model and solid Earth rheological model yields the gravitationally self-consistent RSL changes on a global scale and as a function of time. We solve the SLE by means of the SELEN program (Spada and Stocchi, 2007), which uses the pseudo-spectral method (Mitrovica and Peltier, 1991) and includes solid the Earth rotation, the shift of the center of mass of the Earth as well as the migration of coastlines (time-dependent ocean function). We employ a spherically symmetric, radially stratified, deformable but non-compressible, self-gravitating and rotating solid Earth model. The physical and rheological parameters depend on the radius only, which implies that the rheological model is 1D. We assume a purely elastic lithosphere (outer shell) and keep its thickness fixed to 100 km. The mantle is discretized in three layers, which are characterized by a linear Maxwell viscoelastic rheology, and are called, from top to bottom, Upper Mantle (UM), Transition Zone (TZ) and Lower Mantle (LM). We compare the performance of three different mantle viscosity profiles (MVP) that are characterized by an increase of viscosity gradient from top to bottom (see Table 1 for details)

2.2.1 MIS 5e glacioeustatic scenarios

We make use of the existing global ice-sheet model that was generated by De Boer et al. (2014) by using ANICE-SELEN coupled ice-sheet -- sea-level model. The model describes ice-sheets thickness variation for the last 410 ka and consists of a system of four 3-D regional ice-sheet-shelf models (Eurasia, North America, Greenland and Antarctica) that simulate ice flow with a combination of shallow ice and shelf approximations (de Boer et al., 2014). The topography variations that accompany ANICE-SELEN simulations account for the GIA-induced RSL changes that follow from the solution of the SLE (Spada and Stocchi, 2007). In the ANICE-SELEN model, the four regional ice-sheet models and the induced RSL changes, which in turn drive the topographic variations, are run simultaneously and coupled at every time-step. Hence, the four regional ice-sheet models fully and dynamically incorporate all the GIA feedbacks described by the SLE.

We follow the original ice-sheet chronology starting from 410 ka through the MIS 6 glacial maximum and match the end of MIS 6 Eurasia and North America ice sheets's deglaciation at 127 ka. By the same time, the thickness of Greenland and Antarctic Ice Sheets (GrIS and AIS, respectively) are scaled to reach the present-day volume, which implies a eustatic sea level of 0.0 m above present-day sea level. We keep the GrIS and AIS thicknesses constant between 127 and 116 ka. After 126 ka, the four ice sheets follow the original simulation presented in De Boer et al. (2014) and undergo the fourth (and last) glacial-interglacial cycle. We call this model “background model" and the associated GIA response between 127 and 116 ka "background GIA", implying that it accounts for the GIA contribution of the three glacial-interglacial cycles previous to MIS 5e interglacial.

Subsequently, the melting of the GrIS and AIS between 127 and 116 ka is over-imposed to the background model according to the following four scenarios (see Figure 3):

- *Scenario 1.* This scenario reflects the traditional view of MIS 5e sea-level history, with the melting of both GrIS (2.0m) and AIS (5.0m) occurring early in the interglacial, and not changing until insolation in both hemispheres decreases and glacial conditions start to resettle (see Figure 3).
- *Scenario 2.* This scenario includes a two-step highstand. However, the GrIS contributes 2.0 m of ESL equivalent between 127 and 116 ka while the AIS contributes 5.0m only after 120 ka (Figure 3).
- *Scenario 3.* The GrIS and AIS release, respectively, 2.5 and 1.0 m ESL at 127 ka. GrIS remains stable until 116 ka, while AIS releases 4.5 m ESL after 120 ka (Figure 3). The two-step retreat of GrIS and AIS, therefore, results in a maximum eustatic peak of 8.0 m between 119 and 117 ka. Scenarios 2 and 3 are in line with the timing and magnitudes proposed by O'Leary et al. (2013).
- *Scenario 4.* This scenario is chronologically opposite to the scenario and at odds with O'Leary et al. (2013). The GrIS and AIS melt to their maximum extent early in the interglacial, and ice formation is forced in Antarctica towards the end of MIS 5e (Figure 3).

2.2.2 Numerical predictions

We compute, evaluate and discuss *(i)* maximum RSL elevations along a transect that connects the 11 sites of Figure 1, *(ii)* RSL curves at each site, RSL changes across the whole Mediterranean Sea (maps), *(iii)* differences between observed and predicted RSL elevations

3. Results

3.1 RSL data

The difference between the measured elevation of the RSL indicators and the actual paleo sea level can be significant once the indicative meaning is properly accounted for (Figure 2g, see Supplementary Materials for details on the calculation of the indicative meaning at each site and the Supplementary Text for a working example). The set of 11 revised RSL sites from supposedly stable areas in the Mediterranean shows a MIS 5e RSL highstand in the range of 2-10 m above present-day sea level (Figure 2g). Two distinct elevations of the MIS 5e sea level are locally recorded at Mallorca, Tyrrhenian Sea, Sardinia and Tunisia (Figure 2g, sites no.3,5,8 and 9).

3.2 Background GIA in the Mediterranean

The background GIA contributes to a generalized RSL highstand during MIS 5e that is characterized by a significant spatial variability (Figure 4). According to MVP1 (red curve in Figure 4), a maximum RSL elevation of ~2.0 m is predicted at site no. 1 (Al Hoceima, Morocco), while for the other sites the predictions fall within a range of 0.5 and 1.25 m above present-day sea level. The larger gradient between UM and LM viscosity, which characterizes MVP2, yields higher high-stands in the central Mediterranean sites, while the RSL elevation at site no.1 reduces to ~1.3 m (green curve in Figure 4). A further increase in the viscosity gradient UM and LM, as described by MVP3, exacerbates this pattern and results in a higher RSL elevation in the central Mediterranean, while a reduction occurs at sites no.1 and no.11 (blue curve in Figure 4). The absolute maximum high-stand (> 2.0 m) is predicted at sites no.7 and 8 (Sardinia, Italy) for MVP3 (Figure 4). This value is comparable to the glacioeustatic contribution of the GrIS as proposed so far.

The predicted maximum RSL highstands of Figure 4 occur at different times as a function of the geographic location (see Figure 5 a-c). At site no. 1 (Al Hoceima, Morocco; solid red curve in Figure 5a), MVP1 results in a RSL rise ~2.0 m above present-day sea level between 125 and 126 ka. This is followed by a RSL drop that reaches present-day sea level at 116 ka. According to MVP1 and moving eastwards along the transect (i.e. towards the center of the basin), the predicted RSL curves are characterized by lower high-stands that occur later in time. At site no. 4 (Bergeggi, Italy; dotted red curve in Figure 5a) the predicted RSL exceeds present-day sea level after 125 ka.

i.e. 2.0 ka later than at site no. 1, while the maximum elevation occurs 3.0 ka later. At site no. 5 (Cala Mosca, Sardinia, Figure 5a) the predicted maximum RSL elevation occurs by 116 ka. Results for MVP2 show a reduction of the maximum RSL elevation at western and eastern sites and steeper RSL curves (i.e. higher RSL rates; Figure 5b). According to MVP3, the maximum elevation is attained at site 8 (Cala Mosca, Sardinia) at 116 ka (dashed curve in Figure 5c), while site no.1 experiences a high-stand peak that is half the MVP1 prediction and that occurs 6-7 ka later (solid curve in Figure 5c).

To investigate the role of the water-loading term and its interaction with the solid Earth we perform the same simulations of Figures 4 and 5 but neglecting the ice-loading contribution for the whole background model (Background GIA – Ocean loading, see Figure 6a). Therefore, when ice sheets grow (or shrink), water is taken from (or placed to) the oceans without being compensated by ice loads on the continents. The predicted maximum RSL elevations are largely different from the standard background GIA solutions (Figure 6a). The spatial variability of the RSL change is significantly reduced. The sites located in the center of the basin (no.3, and no.5-8) together with the three sites along North Africa (no.9-11) experience a maximum RSL rise that is close to the eustatic value (i.e. 0.0 m above present-day sea level). A maximum RSL elevation of ~0.5 m is predicted at sites no.7 and 8 (Sardinia) for MVP1 (red dots in Figure 6). The maximum elevation decreases with the increasing viscosity gradient between UM and LM in MVP2 and MVP3. This trend is generally opposite to the standard background GIA, where the maximum RSL elevation is calculated for MVP3 (see Figure 4). The maximum RSL elevations are predicted, with decreasing height, at sites no.1, 2 and 4. Also here, as well as at sites no.7 and 8, the viscosity profile has an opposite effect with respect to the standard background GIA solutions of Figure 4. Similarly to the latter, the maximum RSL elevations occur at different times according to the geographical location (solid curves in Figure 6c-h). At sites no.1 and 4 (Figure 6c and d, respectively), the maximum highstand occurs at 127 ka. which corresponds to the end of MIS 6 ice-sheets deglaciation. For all the three mantle viscosity profiles, the highstands are followed by a RSL drop that closely resemble the standard background GIA prediction for MVP1 at site no.1 (see Figure 5a). Conversely, an almost monotonous RSL rise characterizes the predictions at the central sites no.6 and 8 between 127 and 116 ka (Figure 6e, f). Lower positive RSL rates are predicted at sites no.10 and 11 (Figure 6g, h), where the curves are very close to eustatic.

Neglecting the ice-loading term of the Eurasian aggregate only results in an upward shift of 0.5-1.0 m of the maximum predicted RSL at sites no. 3 and no. 5-11 (Background GIA – Partial ocean loading, see Figure 6b) and with respect to the background GIA – Ocean loading (Figure 6a). At sites no. 1,2 and 3, instead, the maximum elevations are 0.5-1.0 m lower than the background GIA – Ocean loading . The effect of the mantle viscosity profile is in line with the standard background GIA (Figure 4, 5). In fact, the RSL highstand increases in the center of the Mediterranean basin (sites no.3, 7 and 9) when moving from MVP1 to MVP3. The opposite occurs at sites no.1, 2 and 4. The predicted RSL curves at sites no. 1 and 4 are characterized by a lower early highstand peak at 127 ka and by a longer duration of the RSL drop phase (dashed curves in Figure 6c,d). At sites no. 6 and 8 (Figure 6e, f), the ice-loading term results in ~1.0 m highstand between 121 and 116 ka. Similarly to sites no.1 and 4, an early peaked highstand is obtained at sites no. 10 and 11 (Figure 6g, h).

3.3 Scenarios 1-4

Our results account for the background GIA as well as for the GIA that accompanies and follows AIS and GrIS melting during MIS 5e, according to scenarios 1-4 (Figure 3a-d). Figure 7a shows the predicted RSL (with respect to present-day) at 122 ka according to scenario 1 and MVP1. A RSL elevation that is ~0.5-1.0 m higher than eustatic (7.0 m) is already attained by 122 ka along most of the northern coastlines (Figure 7a) and in southern Spain (site no. 2) and Morocco (site no. 1). At sites no. 3, 7 and 8 a maximum value of ~6.0 m is predicted. Therefore, a maximum difference of ~1.5 m is predicted between the coastal areas and the center of the Mediterranean basin, where the background GIA results in a delay in the appearance of the highstand.

Predictions for MVP2 (Figure 7b) and MVP3 (Figure 7c) reveal the role of mantle viscosity profile and, in particular, of the viscosity contrast between UM and LM. According to MVP2, values equal to or 0.5 m higher than the eustatic remain in southeastern Spain and Morocco. At sites no. 3-8 a maximum value of 5-6 m is predicted. Therefore a maximum ~2.5 m difference exists between the center of the Mediterranean basin and the southeastern coasts. This trend increases when moving to MVP3, which in fact results in a further delay of the MIS 5e highstand (Figure 7c).

The predicted RSL curves for scenario 1 and MVP2 show that, by 122 ka (Figure 8), the RSL is dropping at site no. 1, while at sites no. 4, 5, 7 and 8, it is still rising towards the maximum elevation, which then occurs by 116 ka. The predicted RSL trend at site no.1 and between 122 and 116 ka is at odds with the predictions at site no.7. Opposite RSL trends are also predicted at different sites for scenarios 2 and 3 (Figure 8, black and pink curves). This holds in particular between 119 and 117 ka, i.e. after meltwater is released from the AIS (see Figure 3b,c). Both scenarios 3 and 4 result in a maximum highstand peak of 8 m, which occurs between 119 and 117 ka according to scenario 3 and between 127 and 120 ka according to scenario 4.
Our results show that, when scenario 3 is combined with MVP2, the maximum eustatic peak is reached and even surpassed by 119 ka at sites 4, 5, 7 and 10. Instead, the role of background GIA inhibits the appearance of the maximum peak when scenario 4 is considered. This stems from the delayed subsidence of the sea bottom in response to the melting of MIS 6 ice-sheets.

To quantify the differences between predictions and observations we make a heuristic use of the chi-square merit function:

$$\chi^2 = \frac{1}{N}\sum_{i=1}^{N}\frac{\left(S_i^o - S_i^p\right)^2}{\left(\sigma_i^o\right)^2} \qquad \text{Eq. (1)}$$

where *N* is the number of observations, S_i^o is the paleo RSL elevation obtained from field data and considerations on the indicative meaning as described in this paper, σ_i^o is the standard deviation of the observation and S_i^p is the predicted maximum sea level. We first assume that the sea-level observations at the 11 sites considered in this study represent the maximum elevations attained by the sea level during MIS 5e. At the four sites that record two different sea-level stands (Figure 2), we neglect the lower stand and consider the higher elevation only. We predict the highest elevation reached by sea level during MIS 5e according to scenarios 1-4 and MVP 1-3 at each site and then compute the χ^2 (see Eq. 1). Scenario 3 stands out clearly as the worst solution for each of the three mantle viscosity profiles (see Figure 9a). The relatively large misfit mostly stems from the difference between predicted and observed low sea level at site no. 11 (Israel). The latter suggests that each observation does not necessarily correspond to the local maximum highstand attained during MIS 5e. However, the lack of reliable dating techniques prevents a more detailed comparison between data and predictions.

Secondly, we assume that the observed RSL indicators that are below +5.0 m represent a lower highstand, while those above +5.0 m indicate a higher sea-level stand (which might be the maximum MIS 5e local highstand). To locate the events in time we assume that the lower highstands (<= 5.0 m) occurred before120 ka, while the higher occurred after 120 ka. Accordingly, at sites where one sea level only is observed, we assume that it represents either the lower or the higher highstand. At sites where two different sea levels are observed, these record two consecutive highstands. To compare predictions with the observations, we calculate the maximum peaks before and after 120 ka and compare them, respectively, to the lower and higher observed elevations. For Scenario 4 (see Figure 3) we invert the chronological order of the peaks. The comparison between data and predictions (Figure 9b) reveals that scenario 1 is now the least appropriate, being not able to satisfactorily fit a two-step signal. Scenario 3 and 4 are equivalent.

3.4 Tectonic stability from MIS 5e RSL histories

The previous sections show that field data, glacioeustatic scenarios and GIA calculations bring large uncertainties in the reconstruction of MIS 5e sea-level history. These uncertainties must be reflected in tectonic estimates from MIS 5e sea-level observations. In this paragraph we use the field data, GIA and glacioeustatic scenarios (and their uncertainties) described above to answer the question: how significant are field-related, GIA and eustatic sea-level uncertainties when attempting to use MIS 5e shorelines to calculate tectonic vertical deformations?

To answer this question, we use the following equation to calculate uplift/subsidence rates from MIS 5e sea-level histories:

$$PDr = \left[\frac{S_T^o - S_T^p}{T}\right] \qquad \text{Eq. (2)}$$

Where PDr is the post-depositional rate of uplift (positive) or subsidence (negative), S_T^o is the observed paleo RSL (see also Eq. 1), S_T^p is the predicted sea level that stems from Scenarios 1-4 (see Figure 8) and T is time. At each site, we reiterate 1000 solutions of Eq.2 for each time step (each 100 years between 116 and 126 ka, n=11) and for each GIA model and eustatic scenario (n=12), randomly sampling a Gaussian distribution where μ is the paleo RSL at each site and δ is the associated paleo RSL uncertainty to represent S_T^o. We calculate 132,000 possible *PDr* rates, that we plot using simple histograms (blue histograms in Figure 10). We compare this solution with a simpler solution of Eq.2 where, instead of accounting for GIA, we set S_T^p equal to 6 meters, a value often considered as representative of MIS 5e ESL (gray histograms in Figure 10). Although it is possible to affirm that all the 11 sites are characterized by mild rates of tectonic motions, the uncertainties surrounding such assumptions are relevant when GIA and different ESL scenarios are considered (Figure 10).

4. Discussion

Our numerical simulations show that the Earth is not in isostatic equilibrium during the MIS 5e. The GIA processes that accompany and follow the melting of GrIS and AIS during the MIS 5e (scenarios 1-4) add up to the background GIA to increase the regional RSL variability. Each location, within the Mediterranean Sea and during MIS 5e, is characterized by a local RSL curve that can be significantly different from the eustatic.

The GIA-induced spatial variability of the RSL change is small if compared to the vertical tectonic rates (see red and blue squares in Figure 7 a,b,c for southern and northern Italy respectively: sites that are below sea level and above 15 m are considered tectonically active or affected by subsidence because no sensible combination of ESL and GIA can explain such low / high values). However, the GIA signal is significant and definitely non-negligible in the tectonically stable areas (green squares).

The ocean-loading term is an important contributor to the background GIA in the Mediterranean Sea. The central Mediterranean areas are affected by uplift during the MIS 6 glacial maximum in response to water removal. The melt-water redistribution that follows the melting of MIS 6 ice sheets causes subsidence in the bulk of the basin and results in a monotonous RSL rise during the MIS 5e (Figure 6e,f). An opposite trend affects the marginal areas to the West (Morocco and southern Spain; see sites no.1,2 and 4 of Figure 1, 6), where subsidence occurs during the MIS 6 glacial period and uplift during the MIS 5e. The latter is known as continental levering and describes the upward tilt of the continental margin in response to the ocean-load-induced subsidence of the center of the basin (Clark and Lingle, 1979; Stocchi and Spada, 2007). This process is particularly strong at sites no. 1, 2 and 4 (Figure 6a), which are pushed upwards in response to the water-load-induced central subsidence of the Mediterranean Sea and the Atlantic Ocean.

Overall, the ocean loading-term alone results in a uniform RSL response within the Mediterranean basin. The RSL variability, in fact, is mostly reduced because of the lack of the collapsing forebulge around Fennoscandia. The latter is induced by the Fennoscandian ice-loading term and is characterized by a strong latitudinal dependence. The crustal deformations that accompany the collapse of the forebulge, in fact, decrease from north to south across the Mediterranean.

The inclusion of the ice-loading contribution from the distant ice sheets (North America, Greenland and Antarctica) already results in significantly different RSL curves and in higher maximum RSL elevations (see Figure 6). The predicted RSL curves at sites no.10 and 11 (Figure 6g, h) reveal an interesting feedback from the ice-loading term. The latter, in fact, results in an early highstand (127 ka) that is then followed by RSL drop (compared dashed and solid curves of Figure 6g,h). The reason for this is found in the subsidence of peripheral uplifted forebulges that surrounded the formerly glaciated areas (North America, Greenland and Antarctica) at the MIS 6. As a result, water moves from the far-field areas (such as eastern Mediterranean) towards the forebulge regions in order to conserve the ocean mass. This process is known as ocean syphoning (Mitrovica and Milne, 2002) and usually adds to the continental levering. Stocchi and Spada (2007) have shown that this RSL pattern can be found in the Mediterranean during the late Holocene.

The ocean- and ice-loading terms are characterized by different areal extent and interact with different vertical portions of the mantle. Accordingly, the vertical gradient of viscosity is an important parameter in modulating the GIA signal (Stocchi and Spada, 2007, 2009). Mantle viscosity profiles with higher viscosity contrast tend to delocalize the GIA effects. This is because deformation mainly happens in the upper mantle and so flow deformation – tend to stretch out laterally rather then with depth. So, for the full background GIA, this results in s southwards shift of the collapsing forebulge, which now interferes with the RSL changes in the Mediterranean. As a result, the maximum RSL elevation occurs later and is higher in the center of the basin (sites no. 7, 8).

By comparing the predicted RSL in the Mediterranean Sea with the values expected in the Gulf of Biscay and in the Black Sea we can appreciate the contribution of the ice-loading term to the regional RSL variability (Figure 7). By 122 ka the Gulf of Biscay and the Black Sea are characterized by a sea level that is still 2-3 m below the eustatic (7.0 m). This delay is related to the slow subsidence of the peripheral forebulge that uplifted around the Fennoscandia ice sheet during the MIS 6. The subsidence is characterized by a clear N-S trend.

The data-models comparison shows that the differences between observations and predictions generally decrease when a two-step melting chronology for AIS and GrIS (scenario 2-4) is assumed and the observations divided into two age groups (before and after 122 ka). This implies that the observations do not correspond to the maximum eustatic elevation, do not necessarily record the local maximum RSL elevation, and that the latter does not occur at the same time everywhere in the Mediterranean.

Our results are in line with those obtained by other studies that highlighted the importance of including GIA when calculating tectonics or subsidence from MIS 5e shorelines (Creveling et al., 2015; Simms et al., 2016). We remark that the GIA models we used in this study account for a limited (albeit representative of commonly used solutions) number of mantle viscosities (see Austermann et al., 2017) and a single representation of MIS 6 ice sheet configuration. The latter, if varied, may lead to significant departures in RSL predictions (Sivan et al., 2016; Dendy et al., 2017; Rohling et al., 2017). This result becomes even more interesting when the tectonic rates are extrapolated linearly through time (Figure 11). Although this should be considered as a theoretical exercise, as tectonics are never linear through time, it shows that calculating long-term (e.g. Pliocene) or recent (e.g. Holocene) tectonic stability on the basis of the MIS 5e RSL indicators can only give very general indications and must be used accordingly.

5. Conclusions

1. The observed range of MIS 5e RSL highstand from 11 tectonically stable sites in the Mediterranean is comprised between 2 and 10 m above present msl. The observed hoghstands are not necessarily coeval. Evidences of two MIS 5e RSL stands are found in Mallorca, northern Tyrrhenian coast of Italy, southeastern Sardinia and Tunisia.

2. The GIA-induced RSL changes across the Mediterranean are characterized by a significant regional variability throughout the MIS 5e. The Earth is in isostatic imbalance and a generalized RSL highstand above present sea level is predicted. The maximum highstand elevation of 2-2.5 m, which is locally predicted according to the background GIA only, is comparable to the hypothesized eustatic contribution from the GrIS as well as to the lower limit of the observations.

3. According to GIA, the MIS 5e RSL highstand occurs at different times as a function of the geographical location in the Mediterranean.

3. To precisely quantify the GrIS and AIS retreat during MIS 5e on the basis on RSL data, requires that the maximum extent, thickness and retreat of the MIS 6 ice sheets, and in particular of Fennoscandia, are constrained.

4. A two-step melting chronology where the GrIS and AIS retreat is out of phase is capable of reconciling predictions and observations provided that the GIA processes are included.

5. Neglecting the uncertainties that are related to RSL indicators and GIA may lead to over- or underestimations of local crustal motions even at sites that are considered tectonically stable. As a consequence, we suggest that caution should be exercised when extrapolating long-term tectonic rates from MIS 5e shorelines.

Acknowledgments

AR and TL's research is financially supported by: The Institutional Strategy of the University of Bremen, funded by the German Excellence Initiative [ABPZuK-03/2014]; The ZMT, the Leibniz Centre for Tropical Marine Research. The authors acknowledge USSP Urbino Summer School in Paleoclimatology (Urbino, Italy), MEDFLOOD - Modeling Paleo Processes (INQUA CMP projects 1203P and 1603P), PALSEA (PAGES/INQUA working group) and PAIS 2017 (Trieste, Italy), for the useful discussions. We are grateful to F. Antonioli, L. Carobene, M. Firpo, J.J. Fornós, E. Galili, L. Gomez-Pujol, P.J. Hearty and D. Sivan for field visits, useful discussions and insights on some of the sites mentioned in this text.

References

Angelier, J., J. P. Cadet, G. Delibrias, J. Fourniguet, M. Gigout, M. Guillemin, M. T. Hogrel, C. Lalou, and G. Pierre, 1976, Les déformations du Quaternaire marin, indicateurs néotectoniques. Quelques exemples méditerranéens: Revue de Géographie Physique et de Géologie Dynamique, v. XVIII, p. 427-448.

Antonioli, F, Dai Pra, G, Hearty, P. J., 1988. I sedimenti quaternari nella fascia costiera della Piana di Fondi (Lazio meridionale). Bollettino Societa Geologica Italiana 107, 491–501.

Antonioli, F., Ferranti, L., 1992. Geomorfologia costiera e subacquea e considerazioni paleoclimatiche sul settore compreso tra S. Maria Navarrese e Punta Goloritzé (Golfo di Orosei, Sardegna). G. di Geol. 54, 66–89.

Antonioli, F., D'Orefice, M., Ducci, S., Firmati, M., Foresi, L.M., Graciotti, R., Pantaloni, M., Perazzi, P., Principe, C., 2011. Palaeogeographic reconstruction of northern Tyrrhenian coast using archaeological and geomorphological markers at Pianosa island (Italy). Quat. Int. 232, 31–44.

Antonioli, F., Lo Presti, V., Rovere, A., Ferranti, L., Anzidei, M., Furlani, S., Mastronuzzi, G., Orru, P.E., Scicchitano, G., Sannino, G., Spampinato, C.R., Pagliarulo, R., Deiana, G., de Sabata, E., Sansò, P., Vacchi, M., Vecchio, A., 2015. Tidal notches in Mediterranean Sea: a comprehensive analysis. Quat. Sci. Rev. 119, 66–84. doi:10.1016/j.quascirev.2015.03.016

Antonioli, F., Anzidei, M., Amorosi, A., Lo Presti, V., Mastronuzzi, G., Deiana, G., De Falco, G., Fontana, A., Fontolan, G., Lisco, S., Marsico, A., Moretti, M., Orrù, P.E., Sannino, G.M., Serpelloni, E., Vecchio, A., 2017. Sea-level rise and potential drowning of the Italian coastal plains: Flooding risk scenarios for 2100. Quat. Sci. Rev. 158, 29–43. doi:10.1016/j.quascirev.2016.12.021

Anzidei, M., Lambeck, K., Antonioli, F., Furlani, S., Mastronuzzi, G., Serpelloni, E., Vannucci, G., 2014. Coastal structure, sea-level changes and vertical motion of the land in the Mediterranean. Geol. Soc. London, Spec. Publ. doi:10.1144/SP388.20

Austermann, J., Mitrovica, J.X., Huybers, P., Rovere, A., 2017. Detection of a dynamic topography signal in last interglacial sea level records. Sci. Adv. 3, e1700457.

Bardají, T., Goy, J.L., Zazo, C., Hillaire-Marcel, C., Dabrio, C.J., Cabero, A., Ghaleb, B., Silva, P.G., Lario, J., 2009. Sea level and climate changes during OIS 5e in the Western Mediterranean. Geomorphology 104, 22–37.

Benjamin, J., Rovere, A., Fontana, A., Furlani, S., Vacchi, M., Inglis, R.H.H., Galili, E., Antonioli, F., Sivan, D., Miko, S., Mourtzas, N., Felja, I., Meredith-Williams, M., Goodman-Tchernov, B., Kolaiti, E., Anzidei, M., Gehrels, R., 2017. Late Quaternary sea-level changes and early human societies in the central and eastern Mediterranean Basin: An interdisciplinary review. Quat. Int. 449, 29–57. doi:10.1016/j.quaint.2017.06.025

Carobene, L., 2015. Marine Notches and Sea-Cave Bioerosional Grooves in Microtidal Areas : Examples from the Tyrrhenian and Ligurian Coasts — Italy. J. Coast. Res. 31, 536 – 556. doi:10.2112/JCOASTRES-D-14-00068.1

Clark, J.A., Lingle, C.S., 1979. Predicted relative sea-level changes (18 000 years BP to present) caused by late-glacial retreat of Antarctic ice sheet. Quaternary Research, 11, 279-298.

Creveling, J.R., Mitrovica, J.X., Hay, C.C., Austermann, J., Kopp, R.E., 2015. Revisiting tectonic corrections applied to Pleistocene sea-level highstands. Quat. Sci. Rev. 111, 72–80. doi:10.1016/j.quascirev.2015.01.003

De Boer, B., Stocchi, P., Van De Wal, R., others, 2014. A fully coupled 3-D ice-sheet-sea-level model: algorithm and applications. Geosci. Model Dev. 7, 2141–2156.

Deconto, R.M., Pollard, D., 2016. Contribution of Antarctica to past and future sea-level rise. Nature 531, 591–597. doi:10.1038/nature17145

Dendy, S., Austermann, J., Creveling, J.R., Mitrovica, J.X., 2017. Sensitivity of Last Interglacial sea-level high stands to ice sheet configuration during Marine Isotope Stage 6. Quat. Sci. Rev. 171, 234–244. doi:10.1016/j.quascirev.2017.06.013

Düsterhus, A., Rovere, A., Carlson, A.E., Horton, B.P., Klemann, V., Tarasov, L., Barlow, N.L.M., Bradwell, T., Clark, J., Dutton, A., Gehrels, W.R., Hibbert, F.D., Hijma, M.P., Khan, N., Kopp, R.E., Sivan, D., Törnqvist, T.E., 2016. Palaeo-sea-level and palaeo-ice-sheet databases: problems, strategies, and perspectives. Clim. Past 12, 911–921. doi:10.5194/cp-12-911-2016

Dutton, A., Lambeck, K., 2012. Ice Volume and Sea Level During the Last Interglacial. Science 337, 216–219. doi:10.1126/science.1205749

Dutton, A., Carlson, A.E.E., Long, A.J.J., Milne, G.A.A., Clark, P.U.U., DeConto, R., Horton, B.P., Rahmstorf, S., Raymo, M.E., 2015. Sea-level rise due to polar ice-sheet mass loss during past warm periods. Science 349, aaa4019-aaa4019. doi:10.1126/science.aaa4019

Faccenna, C., Becker, T.W., Auer, L., Billi, A., Boschi, L., Brun, J.P., Capitanio, A.A., Funicello, F., Horvàt, F., Jolivet, L., Piromallo, C., Royden, L., Rossetti, F., and Serpelloni, E., 2014.

Mantle dynamics in the Mediterranean. Reviews of Geophysics, doi:10.1002/2013RG000444

Farrell, W.E., Clark, J.A., 1976. On postglacial sea level. Geophys. J. Int. 46, 647–667. doi:10.1111/j.1365-246X.1976.tb01252.x

Federici, P.R., Pappalardo, M., 2006. Evidence of Marine Isotope Stage 5.5 highstand in Liguria (Italy) and its tectonic significance. Quat. Int. 145–146, 68–77.

Ferranti, L., Antonioli, F., Mauz, B., Amorosi, A., Dai Pra, G., Mastronuzzi, G., Monaco, C., Orrù, P., Pappalardo, M., Radtke, U., Renda, P., Romano, P., Sansò, P., Verrubbi, V., 2006. Markers of the last interglacial sea-level high stand along the coast of Italy: Tectonic implications. Quat. Int. 145–146, 30–54.

Galili, E., Zviely, D., Ronen, A., Mienis, H.K., 2007. Beach deposits of MIS 5e high sea stand as indicators for tectonic stability of the Carmel coastal plain, Israel. Quat. Sci. Rev. 26, 2544–2557. doi:10.1016/j.quascirev.2007.06.027|ISSN 0277-3791

Goy, J. L., C. Zazo, T. Bardaji, L. Somoza, C. Causse, and C. Hillaire Marcel, 1993, Eléments d'une chronostratigraphie du Tyrrhénien des régions d'Alicante-Murcie, Sud-Est de l'Espagne: Geodinamica Acta, v. 6, p. 103-119.

Graciotti, R., Foresi, L.M., Pantaloni, M., 2002. Caratteristiche geomorfologiche dell'Isola di Pianosa (Arcipelago toscano). Atti Soc. toscana di Sci. Nat. Mem., Ser. A 108, 95–111.

Hearty, P.J., 1986. An inventory of last interglacial (s.l.) age deposits from the Mediterranean basin: a study in isoleucine epimerization and U-series dating. Zeitschrift fur Geomorphol. Supplement, 62, 51–69.

Hearty, P.J., Hollin, J.T., Neumann, a. C., O'leary, M.J., McCulloch, M., O'Leary, M.J., 2007. Global sea-level fluctuations during the Last Interglaciation (MIS 5e). Quat. Sci. Rev. 26, 2090–2112. doi:10.1016/j.quascirev.2007.06.019

Hibbert, F.D., Rohling, E.J., Dutton, A., Williams, F.H., Chutcharavan, P.M., Zhao, C., Tamisiea, M.E., 2016. Coral indicators of past sea-level change: A global repository of U-series dated benchmarks. Quat. Sci. Rev. 145, 1–56. doi:10.1016/j.quascirev.2016.04.019

Hijma, M.P., Engelhart, S.E., Törnqvist, T.E., Horton, B.P., Hu, P., Hill, D.F., 2015. A protocol for a geological sea-level database, in: Shennan, I., Long, A.J., Horton, B.P. (Eds.), Handbook of Sea-Level Research. Wiley Online Library, pp. 536–553. doi:10.1002/9781118452547.ch34

Lambeck, K., Purcell, A., 2005. Sea-level change in the Mediterranean Sea since the LGM: model predictions for tectonically stable areas. Quaternary Science Reviews, 24, 1969-1988.

Lorscheid, T., Stocchi, P., Casella, E., Gómez-Pujol, L., Vacchi, M., Mann, T., Rovere, A., 2017. Paleo sea-level changes and relative sea-level indicators: Precise measurements, indicative meaning and glacial isostatic adjustment perspectives from Mallorca (Western Mediterranean). Palaeogeogr. Palaeoclimatol. Palaeoecol. 473, 94–107. doi:10.1016/j.palaeo.2017.02.028

Mauz, B., Antonioli, F., 2009. Comment on “Sea level and climate changes during OIS 5e in the Western Mediterranean” by T. Bardají, J.L. Goy, J.L., C. Zazo, C. Hillaire-Marcel, C.J. Dabrio, A. Cabero, B. Ghaleb, P.G. Silva, J. Lario, Geomorphology 104 (2009), 22–37. Geomorphology 110, 227–230.

Mauz, B., Fanelli, F., Elmejdoub, N., Barbieri, R., 2012. Coastal response to climate change: Mediterranean shorelines during the Last Interglacial (MIS 5). Quat. Sci. Rev. 1–10.

Mitrovica, J.X., Peltier, W.R., 1991. On postglacial geoid subsidence over the equatorial oceans. J. Geophys. Res. Solid Earth 96, 20053–20071. doi:10.1029/91JB01284

Mitrovica, J.X., Milne, G.A., 2002. On the origin of late Holocene sea-level highstands within equatorial ocean basins. Quat. Sci. Rev. 21, 2179–2190.

Muhs, D.R., Simmons, K.R., Meco, J., Porat, N., 2015. Uranium-series ages of fossil corals from Mallorca, Spain: The “Neotyrrhenian” high stand of the Mediterranean Sea revisited. Palaeogeogr. Palaeoclimatol. Palaeoecol. 438, 408–424. doi:10.1016/j.palaeo.2015.06.043

Murray-Wallace, C. V, Belperio, A.P., 1991. The last interglacial shoreline in Australia—a review. Quat. Sci. Rev. 10, 441–461.

O'Leary, M.J., Hearty, P.J., Thompson, W.G., Raymo, M.E., Mitrovica, J.X., Webster, J.M., 2013. Ice sheet collapse following a prolonged period of stable sea level during the last interglacial. Nat. Geosci. 6, 796–800. doi:10.1038/ngeo1890

Paskoff, R., Sanlaville, P., 1983. Les cotes de la Tunisie: variations du niveau marin depuis le Tyrrhenien. Collect. LA MAISON L'ORIENT MÉDITERRANÉEN 14.

Pedoja, K., Husson, L., Johnson, M.E., Melnick, D., Witt, C., Pochat, S.S., Nexer, M.M., Delcaillau, B., Pinegina, T., Poprawski, Y., Authemayou, C., Elliot, M., Regard, V., Garestier, F., 2014. Coastal staircase sequences reflecting sea-level oscillations and tectonic uplift during the Quaternary and Neogene. Earth-Science Rev. 132, 13–38. doi:10.1016/j.earscirev.2014.01.007

Peltier, W.R., 2004. Global glacial isostasy and the surface of the ice-age Earth: The ICE-5G (VM2) model and GRACE. Annu. Rev. Earth Planet. Sci. 32, 111–149.

Raymo, M.E., Mitrovica, J.X., O'leary, M.J., DeConto, R.M., Hearty, P.J., 2011. Departures from eustasy in Pliocene sea-level records. Nat. Geosci. 4, 328–332.

Rohling, E.J., Hibbert, F.D., Williams, F.H., Grant, K.M., Marino, G., Foster, G.L., Hennekam, R., de Lange, G.J., Roberts, A.P., Yu, J., Webster, J.M., Yokoyama, Y., 2017. Differences between the last two glacial maxima and implications for ice-sheet, δ18O, and sea-level reconstructions. Quat. Sci. Rev. 176, 1–28. doi:10.1016/j.quascirev.2017.09.009

Rovere, A., Antonioli, F., Bianchi, C.N., 2015. Fixed biological indicators, in: Shennan, I., Long, A.J., Horton, B.P. (Eds.), Handbook of Sea-Level Research. Wiley Online Library, pp. 268–280.

Rovere, A., Raymo, M.E., Vacchi, M., Lorscheid, T., Stocchi, P., Gómez-Pujol, L., Harris, D.L., Casella, E., O'Leary, M.J., Hearty, P.J., 2016a. The analysis of Last Interglacial (MIS 5e) relative sea-level indicators: Reconstructing sea-level in a warmer world. Earth-Science Rev. 159, 404–427. doi:10.1016/j.earscirev.2016.06.006

Rovere, A., Stocchi, P., Vacchi, M., 2016b. Eustatic and Relative Sea Level Changes. Curr. Clim. Chang. Reports 2, 221–231. doi:10.1007/s40641-016-0045-7

Shennan, I., 1982. Interpretation of Flandrian sea-level data from the Fenland, England. Proc. Geol. Assoc. 83, 53–63. doi:10.1016/S0016-7878(82)80032-1

Shennan, I., 1989. Holocene crustal movements and sea-level changes in Great Britain. J. Quat. Sci. 4, 77–89. doi:10.1002/jqs.3390040109

Shennan, I., Horton, B., 2002. Holocene land- and sea-level changes in Great Britain. J. Quat. Sci. 17, 511–526.

Shennan, I., Long, A.J., Horton, B.P., 2014. Handbook of Sea-level Research. Wiley Online Library.

Simms, A.R., Rouby, H.H., Lambeck, K., 2016. Marine terraces and rates of vertical tectonic motion: The importance of glacio-isostatic adjustment along the Pacific coast of central North America. Bull. Geol. Soc. Am. 128, 81–93. doi:10.1130/B31299.1

Sivan, D., Sisma-Ventura, G., Greenbaum, N., Bialik, O.M., Williams, F.H., Tamisiea, M.E., Rohling, E.J., Frumkin, A., Avnaim-Katav, S., Shtienberg, G., Stein, M., 2016. Eastern Mediterranean sea levels through the last interglacial from a coastal-marine sequence in northern Israel. Quat. Sci. Rev. 145, 204–225. doi:10.1016/j.quascirev.2016.06.001

Spada, G., Stocchi, P., 2007. SELEN: A Fortran 90 program for solving the "sea-level equation." Comput. Geosci. 33, 538–562.

Stocchi, P., and Spada, G., 2007. Glacio and hydro-isostasy in the Mediterranean Sea: Clark's zones and role of remote ice sheets. Annals of Geophysics, 50, 741-761.

Stocchi, P., and Spada, G., 2009. Influence of glacial isostatic adjustment upon current sea level variations in the Mediterranean. Tectonophysics, 474, 56-68.

Stocker, T.F., Qin, D., Plattner, G.-K., Tignor, M., Allen, S.K., Boschung, J., Nauels, A., Xia, Y., Bex, V., Midgley, P.M., 2013. Climate Change 2013. The Physical Science Basis. Working Group I Contribution to the Fifth Assessment Report of the Intergovernmental Panel on Climate Change-Abstract for decision-makers.

Suess, E., 1906. The Face of the Earth, vol. 2, F. Tempsky, Vienna.

Ulzega, A., Hearty, P.J., 1986. Geomorphology, stratigraphy and geochronology of Late Quaternary marine deposits in Sardinia. Zeitschrift für Geomorphol. Suppl. Bd., 119–129.

Vacchi, M., Marriner, N., Morhange, C., Spada, G., Fontana, A., Rovere, A., Marriner, N., Morhange, C., Spada, G., Fontana, A., 2016. Multiproxy assessment of Holocene relative sea-level changes in the western Mediterranean: variability in the sea-level histories and redefinition of the isostatic signal. Earth Sci. Rev. 155, 172–197. doi:10.1016/j.earscirev.2016.02.002

Van de Plassche, O., 1986. Sea-level research: a manual for the collection and evaluation of data: A manual for the collection and evaluation of data. Springer. doi:10.1007/978-94-009-4215-8_15

Zazo, C., Goy, J.L., Dabrio, C.J., Bardají, T., Hillaire-Marcel, C., Ghaleb, B., González-Delgado, J.-Á., Soler, V., Bardají, T., Hillaire-Marcel, C., Ghaleb, B., González-Delgado, J.-Á., Soler, V., 2003. Pleistocene raised marine terraces of the Spanish Mediterranean and Atlantic coasts: records of coastal uplift, sea-level highstands and climate changes. Mar. Geol. 194, 103–133.

Zazo, C., Goy, J.L.L., Dabrio, C.J.J., Lario, J., González-Delgado, J. a. A., Bardají, T., Hillaire-Marcel, C., Cabero, a., Ghaleb, B., Borja, F., Silva, P.G.G., Roquero, E., Soler, V., 2013. Retracing the Quaternary history of sea-level changes in the Spanish Mediterranean–Atlantic coasts: Geomorphological and sedimentological approach. Geomorphology 196, 36–49. doi:10.1016/j.geomorph.2012.10.020

Figures and Tables captions

Figure 1. Tectonics map of the Mediterranean Sea and geographical locations of the 11 RSL sites that considered in this study. Faults are modified after Faccenna et al. (2014). Site names: 1- Morocco-Al Hoceima; 2- Italy-Pianosa; 3- Spain-Cala Blava; 4- Italy-Bergeggi; 5- Italy-Pianosa; 6- Italy-Pisco Montano; 7- Italy-Cala Luna; 8- Italy-Cala Mosca; 9- Tunisia-Hergla-S; 10- Libia-W Libia; 11- Israel-Nahal Galim.

Figure 2. Geological sketches of some of the eleven MIS 5e Mediterranean sites reviewed in this study (see Figure 1 for location). a) Site 9 - MIS 5e beach deposits, Hergla South, Tunisia (redrawn and adapted from Paskoff and Sanlaville, 1983); b) Site 11 - MIS 5e beach deposits, Nahal Galim,

Israel; c) Site 8 - MIS 5e beach deposits, Cala Mosca, Sardinia, Italy (redrawn from Hearty, 1986); d) Site 6 - Tidal notch and associated deposits, Pisco Montano, Italy; e) Site 3 - MIS 5e beach deposits, Cala Blava, Mallorca, Spain; f) Site 5 – Biological sea level markers and MIS 5e beach deposits, Pianosa, Italy; g) Measured RSL marker (black line) vs paleo RSL elevation (blue band) for all the locations shown in Figure 1 (letters indicate the outcrops described in a-f). References for sites in g): **Site 1** - Angelier et al, 1976; **Site 2** - Mauz & Antonioli, 2009; Bardajii et al., 2009; Zazo et al., 2003; Goy et al., 1993; **Site 3** - Zazo et al., 2003; Zazo et al., 2013; Lorscheid et al., 2015; Hearty, 1986; Muhs et al., 2015; **Site 4** - Carobene et al., 2014; Ferranti et al., 2006; Federici and Pappalardo, 2006; **Site 5** - Antonioli et al., 2011; Graciotti et al., 2002; **Site 6** - Antonioli et al., 1998; **Site 7** - Antonioli & Ferranti, 1992; **Site 8** - Ulzega and Hearty, 1986; Hearty, 1986; **Site 9** - Hearty et al., 2007; Paskoff and Sanlaville, 1983; **Site 10** - Pedoja et al., 2014; **Site 11** - Galili et al., 2007; Mauz et al., 2012.

Figure 3. GrIS and AIS melting scenarios reflecting the uncertainties in MIS5e glacioeustatic contributions (m ESL). See text for the description of each scenario.

Figure 4. Predicted maximum RSL elevation between 127 and 116 ka for the background GIA and according to MVP1 (red), MVP2 (green) and MVP3 (blue). The predicted values are computed along the transect connecting the sites shown in Figure 1 from West to East. Colored squares correspond to the 11 investigated sites mapped in Figure 1.

Figure 5. Predicted RSL curves at each of the 11 sites of Figure 1 according to the background GIA. Red, green and blue colors stem for, respectively, MVP1, 2 and 3 (a-c). Thick solid curve represents site no. 1 (Al Hoceima, Morocco); thick dotted curve represents site no.4 (Bergeggi, Italy); Cala Mosca (Italy); thick dashed curve represents site no.8 (Cala Mosca, Sardinia, Italy). The black thin solid curves represent the remaining 8 sites for the three MVPs and show the spatio-temporal variability of GIA in the area.

Figure 6. The role of ocean- and ice-loading terms. a) predicted maximum RSL elevation according to background GIA and considering the ocean-loading term only (i.e. the ice-loading term is neglected); b) predicted maximum RSL elevation according to background GIA and neglecting the

ice-loading term for the Eurasian ice-sheets aggregate only; c-h) RSL curves at 6 sites according to a (solid curves) and b (dashed curves). See text for explanations.

Figure 7. Predicted RSL elevation at 122 ka according to glacioeustatic scenario 1 and MVP1-3 (a-c). The colored squared indicate the elevation of MIS5e markers (Pedoja et al., 2014). According to the eustatic approximation, scenario 1 would result in a 7.0 m highstand. However, background GIA combined with the GIA that accompanies and follows the melting of GrIS and AIS (scenario 1) results in a regionally varying RSL at 122 ka. According to MVP1, the predicted RSL exceeds the eustatic value along the northern coasts on the Mediterranean basin (a). Moving toward larger viscosity gradients between upper mantle and lower mantle (b-c) results in lower RSL elevation at 122 ka.

Figure 8. Predicted RSL curves at sites no.1, 4, 5, 7 and 10 according to scenario 1 (blue curve), scenario 2 (pink curve), scenario 3 (black curve), scenario 4 (green curve), background GIA (dotted black curve) and for MVP2.

Figure 9. Predictions vs observations: chi-square estimator. a) chi-square as function of mantle viscosity profile and glacioeustatic scenarios (1-3) and using the highest observed sea level (if there is more than one as in sites no.3, 5, 8 and 9) at each RSL site (see Figure 1, 2) and comparing it to the highest predicted RSL; b) same as (a) but assuming that, where there is one observed sea level only, if it is above or below 5.0 m it is the maximum attained sea level after or before 122 ka respectively. Where two sea levels are observed (sites no.3, 5, 8 and 9), the lower one represents the maximum sea level before 122 ka while the higher one represents the maximum sea level after 122 ka. For scenario 4 the order is inverted in order to be consistent with the ice-sheets chronology (higher peak first, then followed by lower peak).

Figure 10. Histograms showing the relative frequency of the post-depositional rates (PDr) calculated for the 11 Mediterranean sites addressed in this study. Blue histograms show the PDr calculated using the GIA+ESL correction presented in this paper. Gray histograms show the PDr calculated using ESL=6m. The last panel on the lower right shows the cumulative relative frequency for all sites. At sites 3,5,8,9 the histograms represent the results of the calculation of PDr using two RSL indicators.

Figure 11. Example of extrapolation of the PDr shown in Figure 10 for two Mediterranean sites: Pianosa (5) and Cala Luna (7). The lower panels represent details of the upper ones. MPWP = Mid Pliocene Warm Period (Raymo et al., 2011). The blue bands represent the maximum-minimum uplift/subsidence calculated using the GIA+ESL predictions, while the dashed bands represent the uplift/subsidence calculated using ESL=6m in Eq. (2).

Table 1. Mantle viscosity profiles (MVP1-3) characterized by different UM, TZ and LM viscosity values. The depth of UM/TZ boundary is 400 km; The depth of TZ/LM boundary is 670 km. The depth of LM/outer core boundary is 3480 km. MVP1 is a simplification of the original VM1 (Peltier, 1996). MVP2 is a simplification of the VM2 profile that is usually employed with the ICE-5G ice-sheet model (Peltier, 2004); MVP3 follows the mantle viscosity profile used by Lambeck et al. (2004).

Figure 1

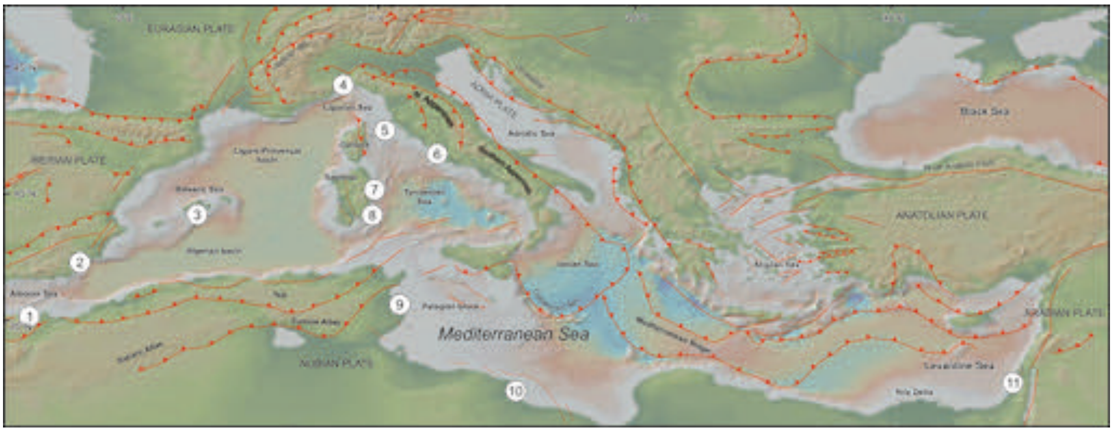
EURASIAN PLATE
IBERIAN PLATE
ADRIA PLATE
Ligurian Sea
Ligurian-Provençal basin
Corsica
Sardinia
Balearic Sea
Algerian basin
Alboran Sea
Tell
Tunisian Atlas
Saharan Atlas
NUBIAN PLATE
Tyrrhenian Sea
Adriatic Sea
Pelagian Shelf
Mediterranean Sea
Ionian Sea
Mediterranean Ridge
Aegean Sea
Black Sea
North Anatolian Fault
ANATOLIAN PLATE
ARABIAN PLATE
Levantine Sea
Nile Delta
1
2
3
4
5
6
7
8
9
10
11

Figure 2

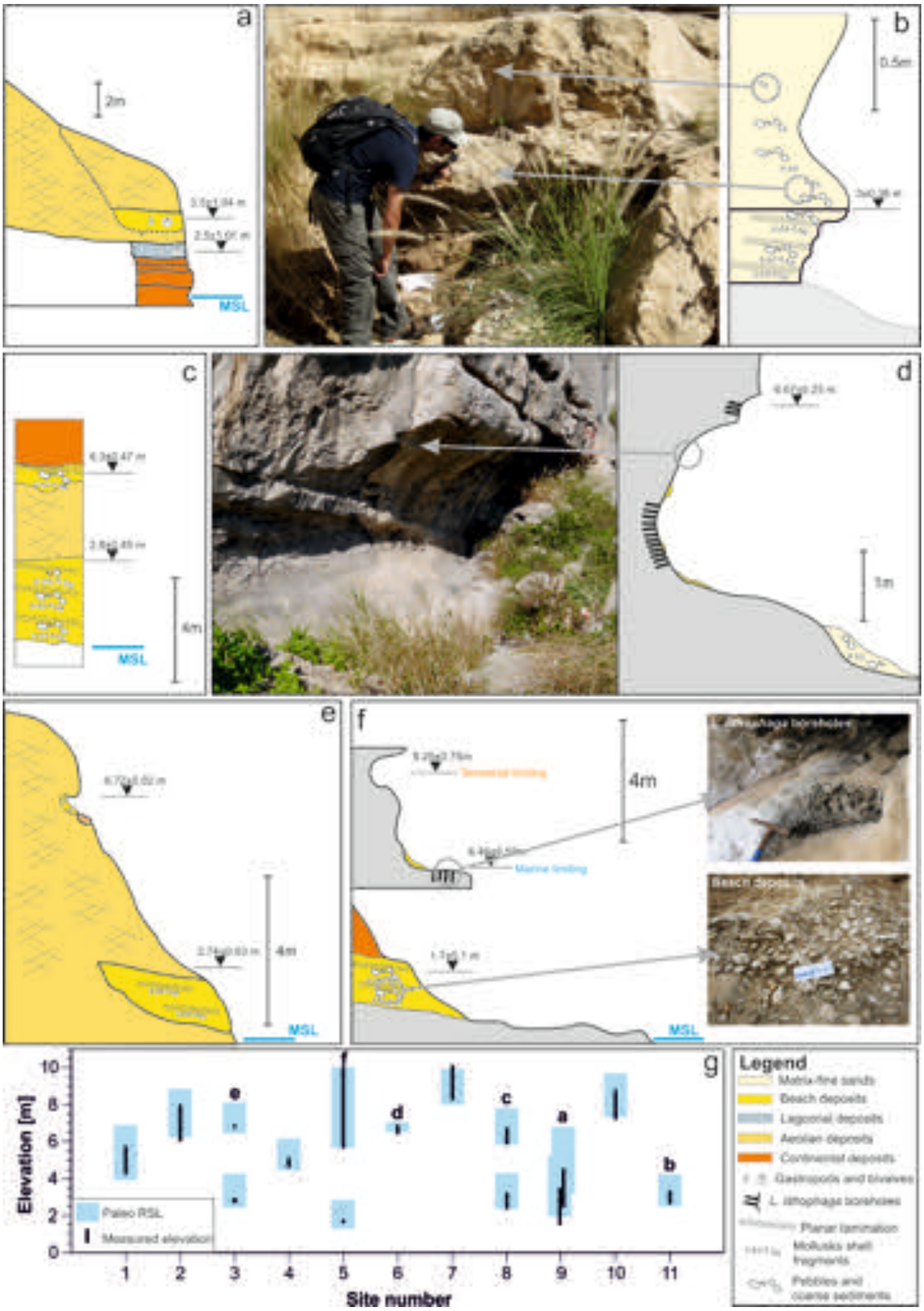
a
2m
MSL
b
0.5m
c
MSL
4m
d
1m
e
4m
MSL
f
4m
Terrestrial limiting
Marine limiting
L. lithophaga boreholes
Beach deposits
MSL
g
Elevation [m]
0
2
4
6
8
10
Site number
1
2
3
4
5
6
7
8
9
10
11
e
f
d
c
a
b
Paleo RSL
Measured elevation
Legend
Matrix-fine sands
Beach deposits
Lagoonal deposits
Aeolian deposits
Continental deposits
Gastropods and bivalves
L. lithophaga boreholes
Planar lamination
Mollusks shell fragments
Pebbles and coarse sediments

Figure 3

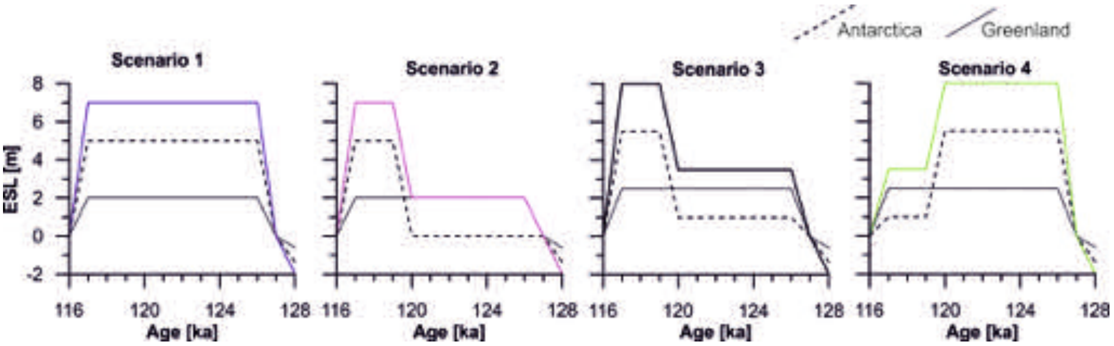
Antarctica
Greenland
Scenario 1
Scenario 2
Scenario 3
Scenario 4
ESL [m]
8
6
4
2
0
-2
116
120
124
128
Age [ka]

Figure 4

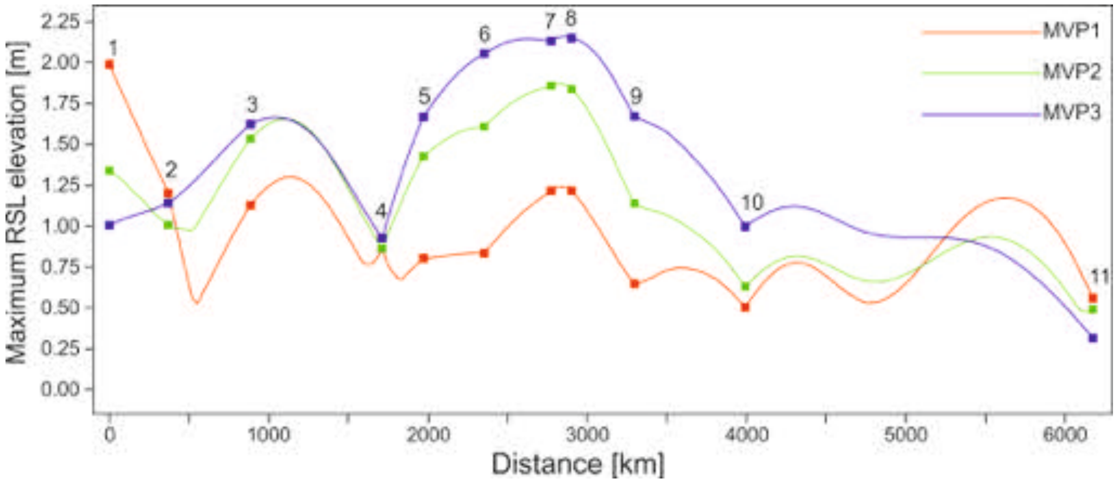
Maximum RSL elevation [m]
0.00
0.25
0.50
0.75
1.00
1.25
1.50
1.75
2.00
2.25
Distance [km]
0
1000
2000
3000
4000
5000
6000
1
2
3
4
5
6
7
8
9
10
11
MVP1
MVP2
MVP3

Figure 5

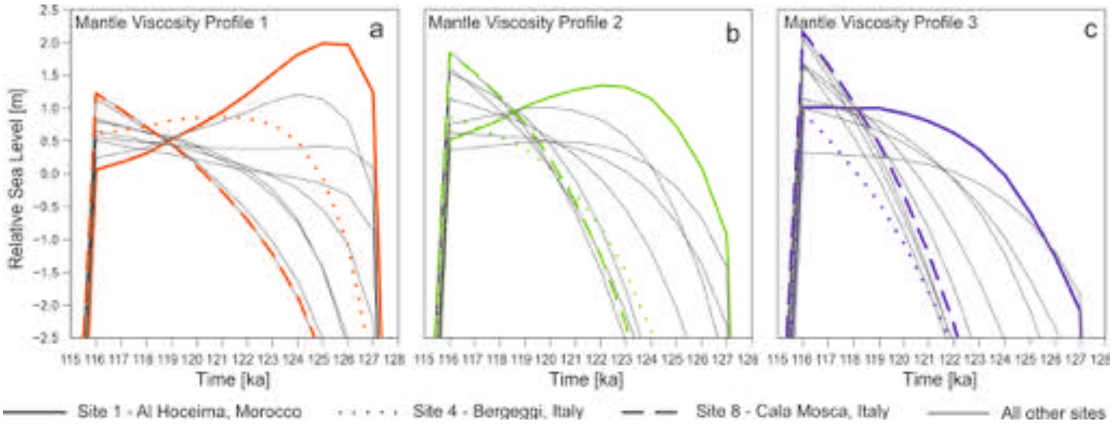
Mantle Viscosity Profile 1
a
Mantle Viscosity Profile 2
b
Mantle Viscosity Profile 3
c
Relative Sea Level [m]
2.5
2.0
1.5
1.0
0.5
0.0
-0.5
-1.0
-1.5
-2.0
-2.5
115 116 117 118 119 120 121 122 123 124 125 126 127 128
Time [ka]
Site 1 - Al Hoceima, Morocco
Site 4 - Bergeggi, Italy
Site 8 - Cala Mosca, Italy
All other sites

Figure 6

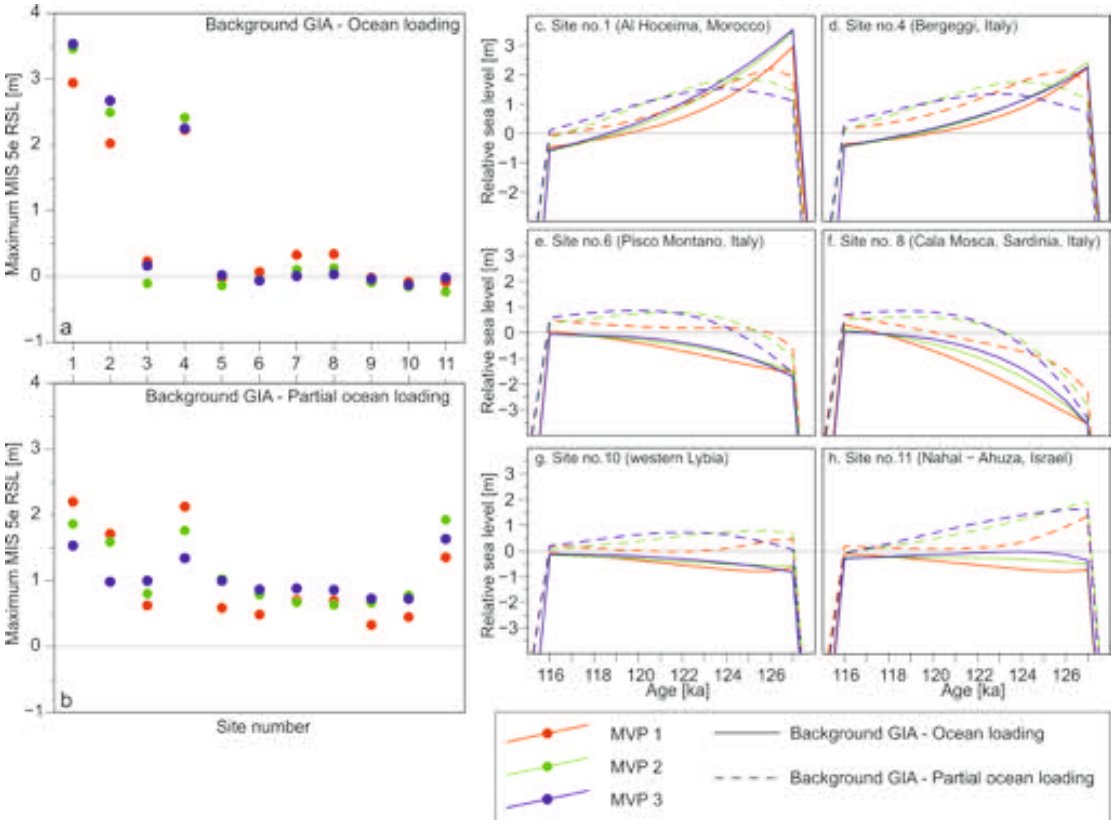
Background GIA - Ocean loading
Maximum MIS 5e RSL [m]
a
Background GIA - Partial ocean loading
b
Site number
c. Site no.1 (Al Hoceima, Morocco)
d. Site no.4 (Bergeggi, Italy)
e. Site no.6 (Pisco Montano, Italy)
f. Site no. 8 (Cala Mosca, Sardinia, Italy)
g. Site no.10 (western Lybia)
h. Site no.11 (Nahal – Ahuza, Israel)
Relative sea level [m]
Age [ka]
116
118
120
122
124
126
MVP 1
MVP 2
MVP 3
Background GIA - Ocean loading
Background GIA - Partial ocean loading

Figure 7

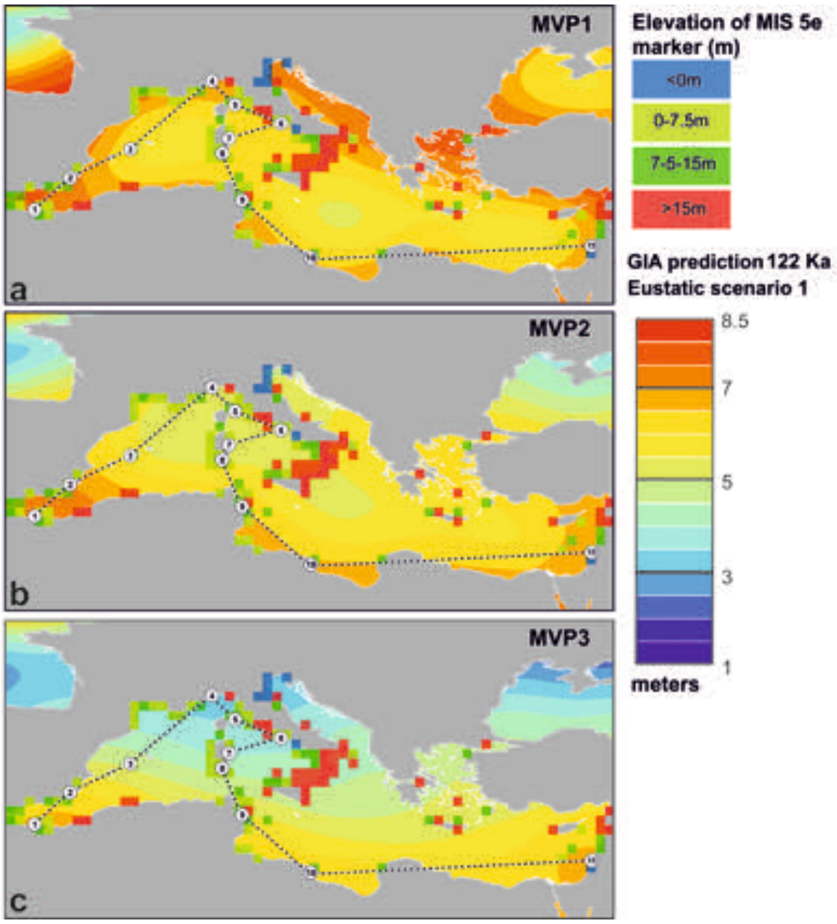
MVP1
MVP2
MVP3
a
b
c
Elevation of MIS 5e marker (m)
<0m
0-7.5m
7-5-15m
>15m
GIA prediction 122 Ka
Eustatic scenario 1
8.5
7
5
3
1
meters

Figure 8

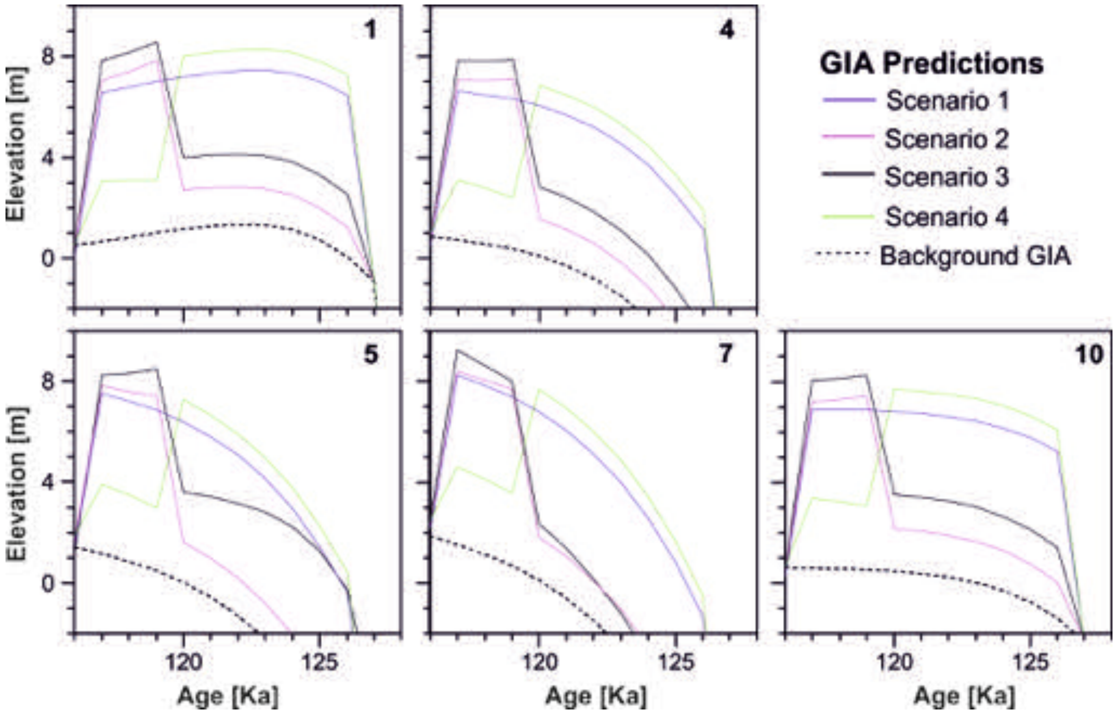
1
4
5
7
10
Elevation [m]
8
4
0
Age [Ka]
120
125
GIA Predictions
Scenario 1
Scenario 2
Scenario 3
Scenario 4
Background GIA

Figure 9

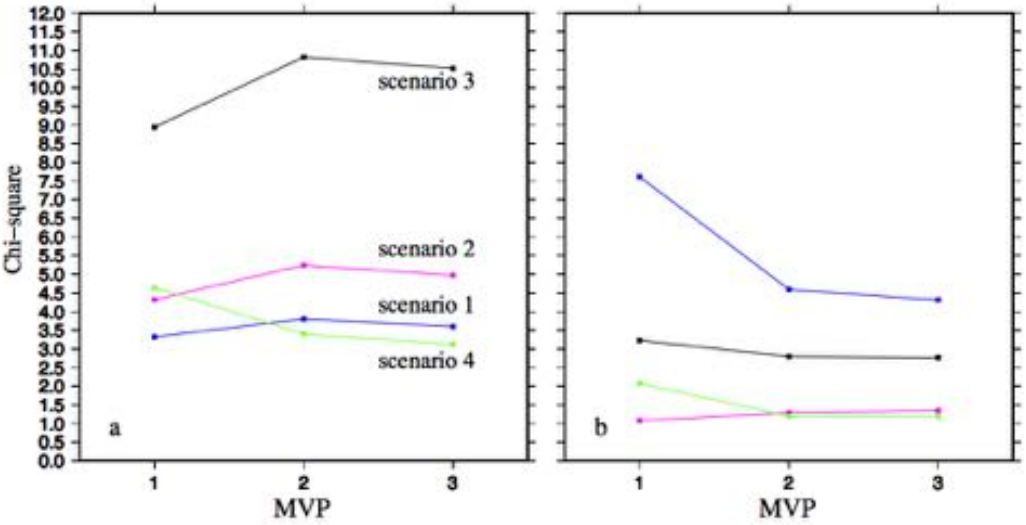
Chi–square
12.0
11.5
11.0
10.5
10.0
9.5
9.0
8.5
8.0
7.5
7.0
6.5
6.0
5.5
5.0
4.5
4.0
3.5
3.0
2.5
2.0
1.5
1.0
0.5
0.0
scenario 3
scenario 2
scenario 1
scenario 4
a
b
1
2
3
MVP
1
2
3
MVP

Figure 10

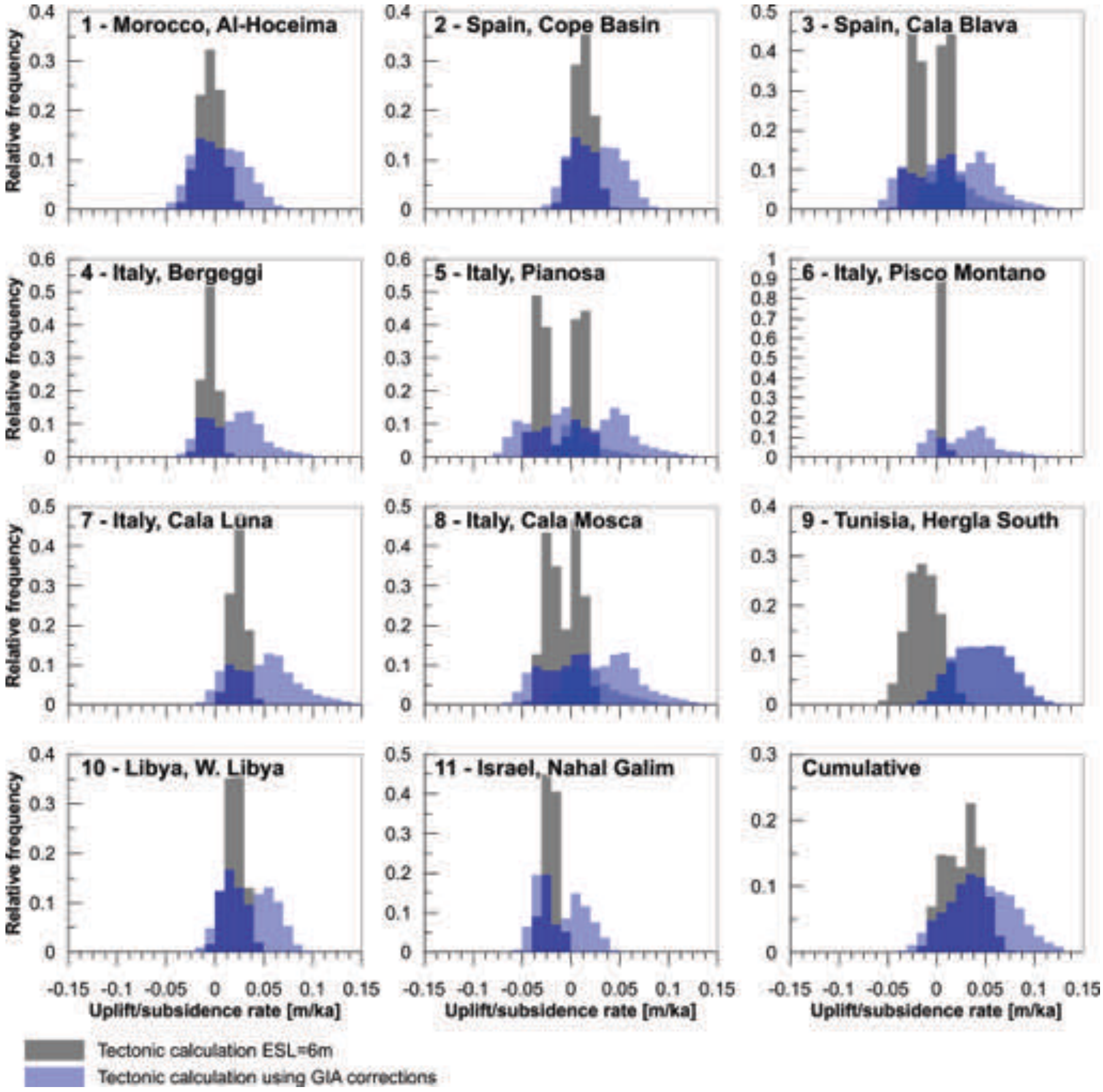
1 - Morocco, Al-Hoceima
2 - Spain, Cope Basin
3 - Spain, Cala Blava
4 - Italy, Bergeggi
5 - Italy, Pianosa
6 - Italy, Pisco Montano
7 - Italy, Cala Luna
8 - Italy, Cala Mosca
9 - Tunisia, Hergla South
10 - Libya, W. Libya
11 - Israel, Nahal Galim
Cumulative
Relative frequency
0
0.1
0.2
0.3
0.4
0.5
0.6
0.7
0.8
0.9
1
-0.15
-0.1
-0.05
0
0.05
0.1
0.15
Uplift/subsidence rate [m/ka]
Tectonic calculation ESL=6m
Tectonic calculation using GIA corrections

Figure 11

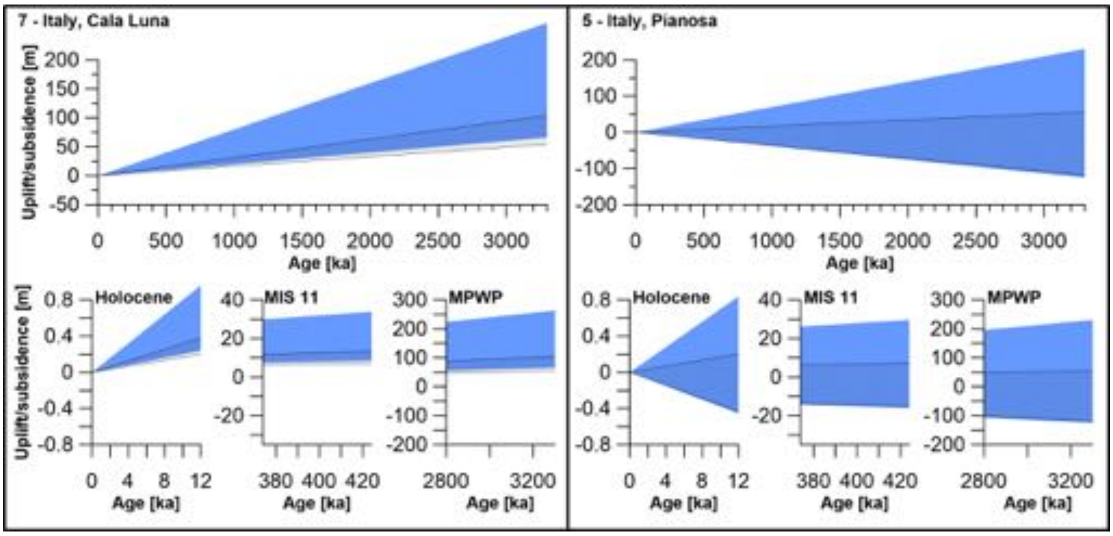
7 - Italy, Cala Luna
Uplift/subsidence [m]
200
150
100
50
0
-50
0
500
1000
1500
2000
2500
3000
Age [ka]
Holocene
0.8
0.4
0
-0.4
-0.8
0
4
8
12
Age [ka]
MIS 11
40
20
0
-20
380
400
420
Age [ka]
MPWP
300
200
100
0
-100
-200
2800
3200
Age [ka]
5 - Italy, Pianosa
200
100
0
-100
-200
0
500
1000
1500
2000
2500
3000
Age [ka]
Holocene
0.8
0.4
0
-0.4
-0.8
0
4
8
12
Age [ka]
MIS 11
40
20
0
-20
380
400
420
Age [ka]
MPWP
300
200
100
0
-100
-200
2800
3200
Age [ka]

Table 1

	UM x10^{21} Pa•s	TZ x10^{21} Pa•s	LM x10^{21} Pa•s
MVP1	1.0	1.0	2.0
MVP2	0.5	0.5	5.0
MVP3	0.25	0.5	10.0